Science of the Total Environment 703 (2020) 135515

Contents lists available at ScienceDirect

Science of the Total Environment

journal homepage: www.elsevier.com/locate/scitotenv

Aggregation-dependent electron transfer via redox-active biochar particles stimulate microbial ferrihydrite reduction

Zhen Yang [a], Tianran Sun [b], Edisson Subdiaga [c], Martin Obst [d], Stefan B. Haderlein [c], Markus Maisch [a], Ruben Kretzschmar [e], Largus T. Angenent [b], Andreas Kappler [a,*]

[a] Geomicrobiology, Center for Applied Geoscience, University of Tuebingen, Germany
[b] Environmental Biotechnology, Center for Applied Geoscience, University of Tuebingen, Germany
[c] Environmental Mineralogy and Chemistry, Center for Applied Geoscience, University of Tuebingen, Germany
[d] Experimental Biogeochemistry, University of Bayreuth, Germany
[e] Soil Chemistry Group, Institute of Biogeochemistry and Pollutant Dynamics, CHN, ETH, Zurich, Switzerland

HIGHLIGHTS

- Small particle size biochar and high biochar:ferrihydrite (Fh) ratios stimulate microbial Fe(III) reduction .
- A certain biochar/Fh ratio is necessary for a close aggregation of the redox active components .
- A close aggregation of cells, biochar, and Fh favors electron transfer from cells to Fh via redox-active functional groups of biochar and conductive biochar carbon matrices.

GRAPHICAL ABSTRACT

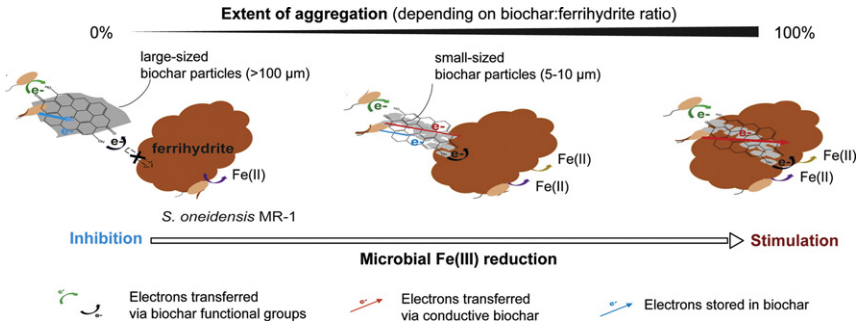

ARTICLE INFO

Article history:
Received 9 September 2019
Received in revised form 11 November 2019
Accepted 12 November 2019
Available online 14 November 2019

Editor: Fang Wang

Keywords:
Biochar
Ferrihydrite
Dissimilatory iron reduction
Electron transfer
Redox mediator
Aggregation

ABSTRACT

Microbial Fe(III) reduction plays an important role for biogeochemical carbon and iron cycling in sediments and soils. Biochar is used as a soil amendment to increase fertility and lower N_2O/CO_2 emissions. It is redox-active and can stimulate microbial Fe(III) mineral reduction. It is currently unknown, however, how the aggregation of cells and Fe(III) minerals with biochar particles influence microbial Fe(III) reduction. Therefore, we determined rates and extent of ferrihydrite (Fh) reduction in *S. oneidensis* MR-1 cell suspensions with different particles sizes of wood-derived Swiss biochar and KonTiki biochar at different biochar/Fh ratios. We found that at small biochar particle size and high biochar/Fh ratios, the biochar, MR-1 cells and Fh closely aggregated, therefore addition of biochar stimulated electron transfer and microbial Fh reduction. In contrast, large biochar particles and low biochar/Fh ratios inhibited the electron transfer and Fe(III) reduction due to the lack of effective aggregation. These results suggest that for stimulating Fh reduction, a certain biochar particle size and biochar/Fh ratio is necessary leading to a close aggregation of all phases. This aggregation favors electron transfer from cells to Fh via redox cycling of the electron donating and accepting functional groups of biochar and via direct electron transfer through conductive biochar carbon matrices. These findings improve our understanding of electron transfer between microorganisms and Fe(III) minerals via redox-active biochar and help to evaluate the impact of biochar on electron transfer processes in the environment.

* Corresponding author at: Geomicrobiology, Center for Applied Geosciences, University of Tuebingen, Sigwartstrasse 10, D-72076 Tuebingen, Germany.
E-mail address: andreas.kappler@uni-tuebingen.de (A. Kappler).

https://doi.org/10.1016/j.scitotenv.2019.135515
0048-9697/

1. Introduction

Iron is one of the most important redox-active elements in nature, participates in microbial respiration as electron acceptor, and plays an important role in biogeochemical processes in general (Lovley et al., 2004; Kappler and Straub, 2005; Weber et al., 2006; Konhauser et al., 2011). Microbial Fe(III) reduction leads to (trans)formation and dissolution of minerals and controls the retention and release of trace metals and nutrients associated with these minerals (Zachara et al., 2001; Borch et al., 2010; Weber et al., 2009). The main mechanisms of electron transfer from microorganisms to Fe(III) minerals include direct contact of cells to Fe(III) minerals and electron transfer via outer-membrane proteins (Myers and Myers, 2003; Newman, 2005). However, at neutral pH, microbial Fe(III) reduction is limited by the low solubility of Fe(III) minerals (Kappler and Straub, 2005; Weber et al., 2006). Therefore, microorganisms have developed other pathways to transfer electrons to Fe (III) minerals (Shi et al., 2016). This includes the release of chelating agents to solubilize Fe(III) minerals (Shi et al., 2012), conductive cell extensions (pili; called microbial nanowires) (Reguera et al., 2005; Malvankar and Lovley, 2014), and the use of redox-active electron shuttles such as cell-produced flavins or natural organic matter (NOM) (Borch et al., 2010; Lovley et al., 1996; Marsili et al., 2008; Bauer and Kappler, 2009; Fuller et al., 2014; Glasser et al., 2017). Electron shuttles can accept electrons from Fe(III)-reducing bacteria followed by abiotic electron transfer from the reduced shuttles to Fe(III) minerals, chromate, chlorinated or nitroaromatic compounds (Lovley et al., 1996; Bauer and Kappler, 2009; Gescher and Kappler, 2013; Roden et al., 2010).

Biochar, produced by artificial pyrolysis of biomass, was shown to have potential to serve as a soil amendment to increase soil fertility, for carbon sequestration, and to lower CO_2/N_2O emissions, probably caused by changes in microbial community composition (Cayuela et al., 2013; Harter et al., 2014; Deluca et al., 2009; Gul and Whalen, 2016; Hagemann et al., 2017; Lehmann and Joseph, 2015). Recently biochar has also been shown to stimulate electron transfer from bacteria to Fe(III) minerals (Kappler et al., 2014; Klüpfel et al., 2014; Yu et al., 2015; Yuan et al., 2017). Biochar is capable of transferring electrons due to the redox-active surface quinone/hydroquinone groups and the conjugated π-electron system in the condensed polyaromatic carbon ring structures in the carbon matrices (Keiluweit et al., 2010). Biochar redox reactions can therefore occur through i) redox cycling (i.e. accepting and donating of electrons) via redox-active quinone/hydroquinone groups (Klüpfel et al., 2014), ii) storage and release of electrons via the electrical double-layer capacitance of carbon matrices (Sun et al., 2017; Deeke et al., 2012; Ji et al., 2014Sudirjo et al., 2019)Sudirjo et al., 2019, and iii) direct electron transfer through the electrical conductance of carbon matrices (Sun et al., 2017; Sun et al., 2018). After addition to soils, biochar will be gradually broken down to small particles in the μm- to mm-size range by physical and chemical weathering as well as microbial decomposition (Lehmann and Joseph, 2015; Nguyen et al., 2008). These small biochar particles can easily be transported through different soil layers (Wang et al., 2013; Zhang et al., 2010) and aggregate with microbes (Gouveia and Pessenda, 2000) and minerals (Ye et al., 2016). It has been shown that smaller powdered biochar particles caused higher rates of microbial Fe(III) reduction compared to larger granulated biochar (Zhou et al., 2017). However, it remained unclear whether and how aggregation of biochar and microbes with Fe(III) minerals influence the electron transfer across the respective solid interfaces, and which mechanism, i.e. electron transfer via redox-active functional groups or via carbon matrices in biochar, dominates the electron transfer during stimulation of microbial Fe(III) reduction.

Probing the dependency of microbial Fe(III) reduction on the aggregation with biochar helps to better understand the electron transfer fundamentals among the three phases and provide practical guidelines for the implementation of biochar particles in soil. The present study therefore investigated the dependency of the rate and extent of microbial ferrihydrite reduction on biochar-cell-ferrihydrite aggregation at different biochar particle size and biochar/ferrihydrite ratios. We used *Shewanella oneidensis* MR-1 as a model Fe(III)-reducing bacterium. *S. oneidensis* MR-1 is an important dissimilatory Fe(III)-reducing bacterium which is ubiquitous in freshwater, marine, soil and sedimentary environments. This strain has been used in various electron shuttling and Fe(III) mineral reduction studies, including experiments with ferrihydrite and biochar (Kappler et al., 2014). We employed light/fluorescence microscopy to analyze the aggregates as well as voltammetry and electron balance calculations to reveal the primary pathways for interfacial electron transfer. We hypothesized that aggregation influences the phase contact between biochar and minerals leading to either stimulation or inhibition of microbial Fh reduction.

2. Materials and methods

2.1. Preparation of biochar suspensions and biochar leachates

Swiss biochar (s-biochar, Belmont-sur-Lausanne, VB, Switzerland) was produced from mixed wood waste materials and KonTiki biochar (k-biochar) from pine wood chips at 700 °C. Due to similar source material (wood chips), the elemental composition of the two biochars was similar (Hagemann et al., 2017). Different particle sizes of biochar were produced by milling (Pulverisette, zirconium oxide balls, Fritsch, Idar-Oberstein, Germany) leading to large-, medium- and small-sized biochars (properties shown in Table S1 and Fig. S3) corresponding to environmentally relevant particle sizes of 100 nm to ca. 150 μm (Wang et al., 2013; Zhang et al., 2010; Song et al., 2019). The milling process results in increased specific surface area of biochar. Compared to the initial biochar particles (200 and 102 m^2/g for s-biochar and k-biochar, respectively), the biochar particles milled showed an increase in specific surface area (Table S1). Anoxic biochar suspensions were prepared as described in the SI.

2.2. Mediated electrochemical analysis

Degassed biochar powders with different particle sizes were suspended in 0.1 M anoxic phosphate buffer (pH 7; final concentration 1 g biochar/L). Electrochemical analysis of biochar suspensions was conducted as published (Xu et al., 2016; Kappler et al., 2014) recently and as described in the SI.

2.3. Fe(III) mineral reduction experiments

Microbial Fe(III) reduction experiments were set up in triplicate in 16 mL glass tubes containing 7.2 mL of 30 mM bicarbonate buffer (pH 7), Fh (0.67, 1.0 1.5, 5, 7.5 and 15 mM Fe as Fh) synthesized according to Amstaetter et al. (2012) as electron acceptor, sodium lactate (3 or 30 mM), and 500 μL biochar suspension at different final concentrations of 1, 5, and 10 g/L, amended with 2×10^9 *S. oneidensis* MR-1 cells/mL (cultivated as described in (Kappler et al., 2014). Anthraquinone-2,6-disulfonate (AQDS, 100 μM) was used as a positive control for electron shuttling to evaluate the effect of biochar amendments on Fe(III) reduction. Abiotic control experiments contained biochar and Fh without MR-1 cells. An experiment using DAX-8 resin particles was done as control for non-conductive but similar-sized particles as the biochars. The effect of biochar leachates on microbial Fh reduction (Fig. S10) was determined using cell suspension experiments with bicarbonate buffer (30 mM), *S. oneidensis* MR-1 (2×10^9 cells/mL), Fh (15 mM), lactate (30 mM), and 0.5 mL of biochar leachates. Biochar toxicity was evaluated in a MR-1 Fe(III) reduction cell suspension experiment with bicarbonate buffer (30 mM), Fe(III)-citrate (5 mM), lactate (30 mM), and biochar (1, 5, and 10 g/L) (Fig. S11).

2.4. Analytical methods

Surface functional groups of s-biochar and k-biochar with different particle sizes were analyzed by Fourier Transform Infrared Spectroscopy (FTIR, IR-Tracer-100, Shimadzu). TOC of freeze-dried biochar powder and DOC in biochar leachates were determined with a TOC analyzer (Analytik Jena, Germany). Biochar particle size was determined by laser diffraction (Malvern Mastersizer 2000). Total Fe(II) (soluble in 1 M HCl) and Fe(tot) (soluble in 1 M hydroxylamine hydrochloride, HAHCl) were determined using the ferrozine assay (Amstaetter et al., 2012; Stookey, 1970). The protein and polysaccharide contents of EPS were quantified using established protocols (Frølund et al., 1996; Zhang et al., 2013). Cell-mineral-biochar aggregates were visualized by bright field and fluorescence microscopy (Leica DM 5500B, Leica, Germany). *S. oneidensis* MR-1 cells were stained by DNA dye Syto 9 combined with propidium iodide, excited at 488 nm). The three-dimensional aggregation of *S. oneidensis* MR-1, Fh and s-biochar was visualized by Confocal Laser-Scanning Microscopy (CLSM, Leica TCS SPE, Leica, Germany). The mineral identity and Fe(II)/Fe(III) content of minerals formed were determined by Mössbauer spectroscopy (Byrne et al., 2016). The zeta potentials of biochar particles (at pH 7, $NaHCO_3$ buffer) were determined by laser Doppler velocimetry (zetasizer, Malvern Nano ZSP) and applying Smoluchowski's equation to convert eletrophoretic mobility into zeta potential values.

2.5. Statistical analysis

Differences between treatments were analyzed by ANOVA using Tukey's test for mean values ($p < .05$). All statistical analyses were carried out using SPSS Statistics 22.0.

3. Results and discussion

3.1. Redox properties of biochars

To evaluate the redox properties of s-biochar and k-biochar, electron accepting capacity (EAC) and electron donating capacity (EDC) were quantified by mediated electrochemical analysis (Klüpfel et al., 2014) for large-sized particles (LP, main fraction > 100 μm), intermediate-sized particles (MP, small fraction 0.1–0.5 μm and main fraction 10–20 μm), and small-sized particles (SP, small fraction 0.1–0.3 μm and main fraction 5–10 μm) biochar (Fig. S1). The EAC values of all biochar particles were 0.752 ± 0.002 to 0.787 ± 0.001 meq e−/g biochar for s-biochar and 0.530 ± 0.001 to 0.589 ± 0.001 meq e−/g biochar for k-biochar, while the EDC values of all biochar particles were 0.231 ± 0.001 to 0.232 ± 0.001 meq e−/g biochar for s-biochar and 0.182 ± 0.002 to 0.184 ± 0.001 meq e−/g biochar for k-biochar (Fig. S1). We found that particle size had no influence on EAC and EDC indicating that the milling process applied to produce different particle sizes did not cause any redox property artifacts. EAC and EDC values determined for s-biochar and k-biochar are similar as determined electrochemically for another wood-derived biochar. (Harter et al., 2014). The redox properties of the biochar depend on the heat treatment temperature (HTT), the general trend is that chars produced at intermediate to high HTTs (400–700 °C) show higher EDC and EAC than that produced at low HTTs (200–300 °C) (Klüpfel et al., 2014). Biochars produced at 700 °C, as our biochars, typically are more oxidized (EAC > EDC). The highest range of EAC values were observed at production temperatures of 500–700 °C (Klüpfel et al., 2014). EAC values of biochar correlate with its quinone content (Klüpfel et al., 2014)[28] suggesting that our s-biochar has more quinone functional groups than the k-biochar. The EEC (sum of EAC and EDC), was calculated for s-biochar and k-biochar to be 0.98–1.02 and 0.71–0.77 meq e^-/g biochar for all particle sizes. These values are higher than EEC values of other wood-derived biochars (0.3–0.7 meq e^-/g) (Klüpfel et al., 2014) but comparable to values of activated carbon (1.34–1.42 meq e^-/g) (Wu et al., 2017). The EECs of biochars normalized to TOC (meq e^-/mg C) (Fig. S2) show that the mixed wood-derived s-biochar has a higher EEC than the k-biochar. The surface functional groups of s-biochar and k-biochar were analyzed by FTIR. Ketones, aromatic carbon, and carboxyl groups were identified by C═C and C═O stretching bonds (1700 cm^{-1} and 1600 cm^{-1}) (Fig. S3). The absence of significant changes in the C═C and C═O stretching bonds between LP and SP of s-biochar and k-biochar indicates that the particle size (the milling process) had no obvious influence on the presence of functional groups in the biochar and confirms the observation that on a per weight basis, all particle sizes have similar EAC/EDC values.

3.2. Microbial Fh reduction rates and extent

We conducted cell suspension experiments with Fh as electron acceptor, *S. oneidensis* MR-1 as Fe(III)-reducing bacterium and different particle sizes and concentrations of biochar (leading to different biochar:Fh ratios) to determine the rates and extent of microbial Fh reduction (Fig. 1; 16-hour long-term experiments are shown in Fig. S5). First Fh reduction experiments were performed with 10 g/L of s-biochar and 15 mM Fe as Fh (Fig. 1A). We found that all biochar particle sizes stimulated Fh reduction; the smaller the biochar particle size, the higher rates and extents of Fh reduction. AQDS has been shown to be an efficient electron shuttling model compound and was used here as exogenous electron shuttle for comparison to biochar (Rau et al., 2002; O'Loughlin, 2008; Jiang and Kappler, 2008; Scott et al., 1998; Benner et al., 2002; Eusterhues et al., 2014). For small-particle s-biochar, the rate and extent of Fh reduction was even higher than with AQDS that significantly stimulated the rate and extent of microbial Fh reduction (ANOVA, $p = .012$) in accordance with previous studies (Lovley et al., 1996; Byrne et al., 2016). Addition of DAX-8 resin particles with particle sizes similar as LP, MP and SP biochar showed no influence on microbial Fh reduction (Fig. S7). Additionally, we found no evidence that surface-attached microbial growth influenced microbial Fh reduction in the presence of DAX-8 suggesting that the positive biochar effect in our experiments is not due to a particle effect but is related to the redox activity of biochar.

In contrast to these first experiments with 10 g/L biochar and 15 mM Fh (biochar/Fh ratio of 0.67 g/mmol Fe), lower biochar concentrations of either 5 or 1 g/L, resulting in lower biochar/Fh ratios of 0.3 and 0.067 g/mmol Fe, inhibited microbial Fh reduction relative to experiments without biochar (Fig. 1B, C, D and Fig. S5). These results suggest an effect of the biochar:Fh ratio on microbial interactions with the biochar particles. To investigate whether a certain ratio of biochar to Fh is required to stimulate microbial Fh reduction, we performed experiments at high biochar/Fh ratios of 0.67, 1.0 and 1.5 g/mmol Fe, respectively, using either 5 or 1 g/L s-biochar (Fig. 2). We found that at a ratio of 0.67 with 5 g/L s-biochar (Fig. 2Aa, 16-hour experiments in Fig. S6), small-particle s-biochar stimulated electron transfer, medium-sized particles had no significant effect (ANOVA, $p = .62$) while large-particle s-biochar significantly slowed down (but did not completely prevent) Fe(III) reduction (ANOVA, $p = .023$) compared to the setup without biochar. When increasing the biochar/Fh ratio to 1.0 g/mmol Fe (with 5 g/L s-biochar), large and medium-sized particles showed no significant effect (ANOVA, $p = .13$) but small-sized particles stimulated (ANOVA, $p = .003$) Fe(II) formation (Fig. 2B). For setups with 1 g/L of s-biochar and a biochar/Fh ratio of 0.67 g/mmol Fe, all biochar particle sizes showed an inhibitory effect on Fh reduction (Fig. 2C). When the biochar/Fh ratio was increased to 1.0 g/mmol Fe with 1 g/L biochar, small-particle s-biochar stimulated Fh reduction, medium-sized s-biochar showed no effect, and large-particle s-biochar inhibited Fe(II) formation (Fig. 2D). At a biochar/Fh ratio of 1.5 g/mmol Fe (with 1 g/L biochar), all biochar particle sizes stimulated microbial Fh reduction (Fig. 2E).

We also determined for k-biochar whether a certain biochar/Fh ratio is required to stimulate microbial Fh reduction (Figs. S8 and S9). When

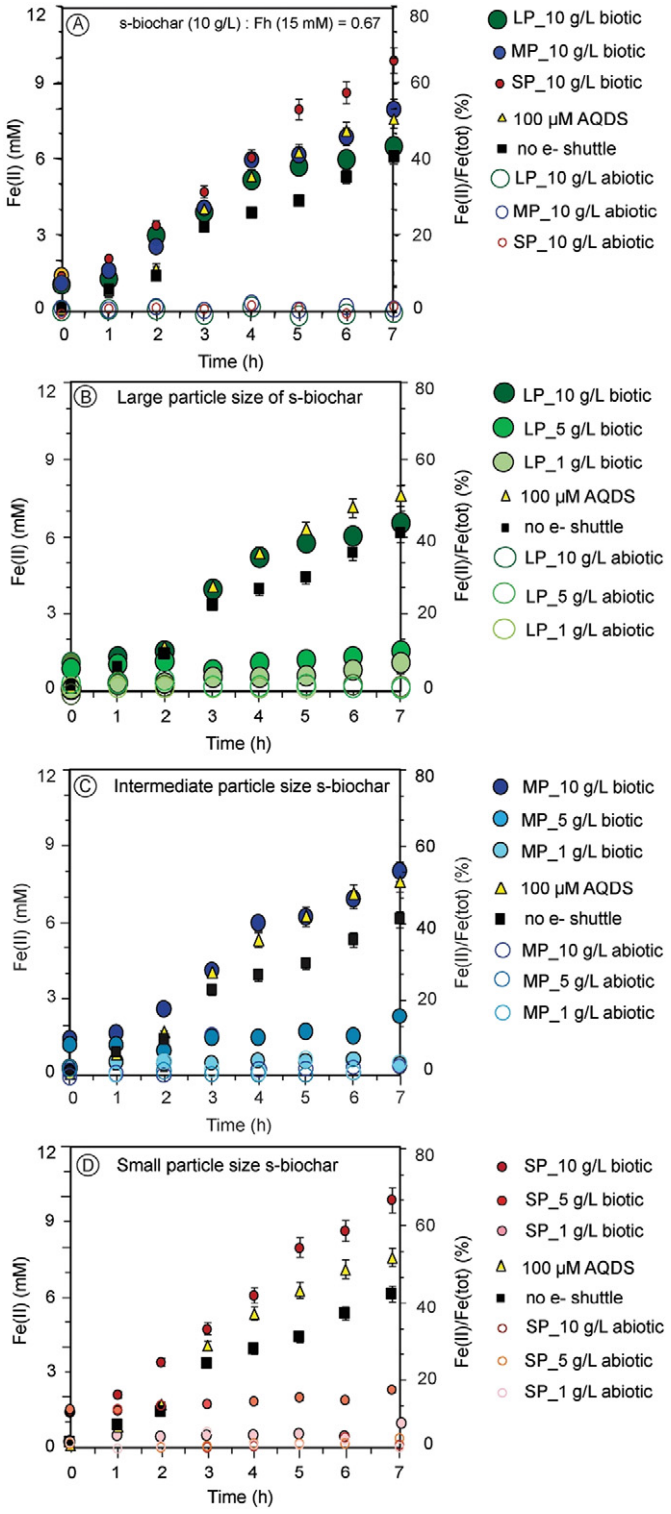

Fig. 1. Microbial ferrihydrite (Fh, 15 mM) reduction by *S. oneidensis* MR-1 in the presence of (A) large, intermediate and small particle size (LP, MP, SP) of Swiss biochar (s-biochar, 10 g/L), (B) 1, 5 and 10 g/L of large particle size s-biochar, (C) 1, 5 and 10 g/L of intermediate particle size s-biochar, and (D) 1, 5 and 10 g/L of small particle size s-biochar. Error bars represent standard deviations of triplicate experimental setups. The results for 16-h incubations are shown in Fig. S5.

using setups with a k-biochar/Fh ratio of 0.67 g/mmol Fe (with 10 g/L k-biochar) or a ratio of 1.0 g/mmol Fe (with 1 g/L k-biochar), all k-biochar particles (LP, MP, and SP) slowed down Fe(II) formation compared to setups without shuttle. In contrast, at ratios of 2.0 g/mmol Fe (with 10 g/L k-biochar), 2.5 g/mmol Fe (with 5 g/L k-biochar) and 3.3 g/mmol Fe (with 1 g/L k-biochar) all three particles sizes of k-biochar stimulated microbial Fh reduction.

In summary these experiments have shown that smaller particle sizes and high biochar:Fh ratios stimulated microbial Fh reduction, while large particles and lower biochar:Fh ratio inhibited reduction relative to controls without biochar suggesting that a certain biochar/Fh ratio was necessary for stimulating Fh reduction (Fig. 2, bottom). For the biochars used in this study, the biochar/Fh ratio played a more important role than particle size for stimulation of microbial Fh reduction. At a certain ratio of biochar/Fh, the s-biochar (due to its higher electron accepting and donating capacity) showed higher rates and extent of microbial Fh reduction than k-biochar.

In a control experiment with 15 mM Fh and MR-1 cells we determined whether biochar leachate, i.e. redox-active molecules mobilized from the biochar particles during incubation in our experiment, had any effects on microbial Fh reduction (Fig. S10). We found that leachates from our biochar (ca. 4.5 mg C/L) did not have any apparent influence on rates and extents of microbial Fh reduction. Our result is in contrast to a previous study (Song et al., 2019) that showed stimulation of microbial Fh mineral reduction by straw-derived biochar leachates (TOC content up to 26.5 mg C/L), but is in agreement with Wu et al. (2017) who showed that the leachate from activated carbon could not enhance Fh reduction. These differences may be rationalized by the low DOC content of our leachate (ca. 4.5 mg C/L) that is lower than the threshold concentration (ca. 5–10 mg C/L) required for electron shuttling (Jiang and Kappler, 2008). Finally, a Fe(III) reduction experiment with Fe(III) citrate (5 mM) and MR-1 cells with and without biochar particles showed that there is no toxic effect of the biochar used in our experiments on the MR-1 cells (Fig. S11).

3.3. Aggregation of S. oneidensis MR-1 cells with biochar and Fh

In the absence of dissolved electron shuttles (neither from biochar leachate nor from the MR-1 cells since they are not producing shuttles in non-growing cell suspensions), electron transfer from the MR-1 cells to Fh depends on the ability of electrons to be transferred either from cells directly to the Fh particles or from cells via redox-active biochar particles to the Fh. Therefore, we monitored aggregates of s-biochar with Fh and MR-1 cells by fluorescence microscopy at different s-biochar/Fh ratios. In setups of small-particle s-biochar with Fh (ratio of 0.67 g/mmol) where stimulation of Fh reduction was observed, the s-biochar particles were associated with the Fh (Fig. 3A) and the cells were attached to both Fh and biochar (Fig. 3B). Overlay images of bright-field and fluorescence images (Fig. 3C) indicated a close association of cells with s-biochar and Fh obviously facilitating electron transfer and therefore stimulating Fh reduction. In contrast, in images with 5 g/L large-particle s-biochar (ratio of 0.3 g/mmol Fe), the s-biochar particles were less associated with Fh (Fig. 3D) and the MR-1 cells were mainly attached to the s-biochar but not to Fh (Fig. 3E). Consequently, these setups showed inhibition of Fh reduction compared to setups without biochar, probably due to limited electron transfer from the cells to the Fh based on the greatly diminished contact with the Fh (Fig. 4F). When keeping the same s-biochar concentration of 5 g/L but with small-particle s-biochar and decreasing the Fh to 5 mM yielding a ratio of 1.0 g/mmol Fe, s-biochar particles showed an intimate association with Fh (Fig. 3G) and MR-1 cells were also associated with both s-biochar and Fh (Fig. 3H and I), suggesting again a close association of cells, Fh and s-biochar thus leading again to stimulation of Fh reduction. While dissolved electron shuttles can also contribute to a stimulation of electron transfer by diffusion, in the case of biochar particles diffusion probably plays a minor role as the biochar rather may act as a solid-state bridge between cells and Fh to accelerate electron transfer (Fig. 3A–C, and G–I). Additionally, these results suggest that MR-1 cell adhesion to biochar that is associated with Fh is necessary for stimulating electron transfer in the presence of biochar as an electron shuttle between MR-1 cells and Fh. Interestingly, a cell suspension experiment

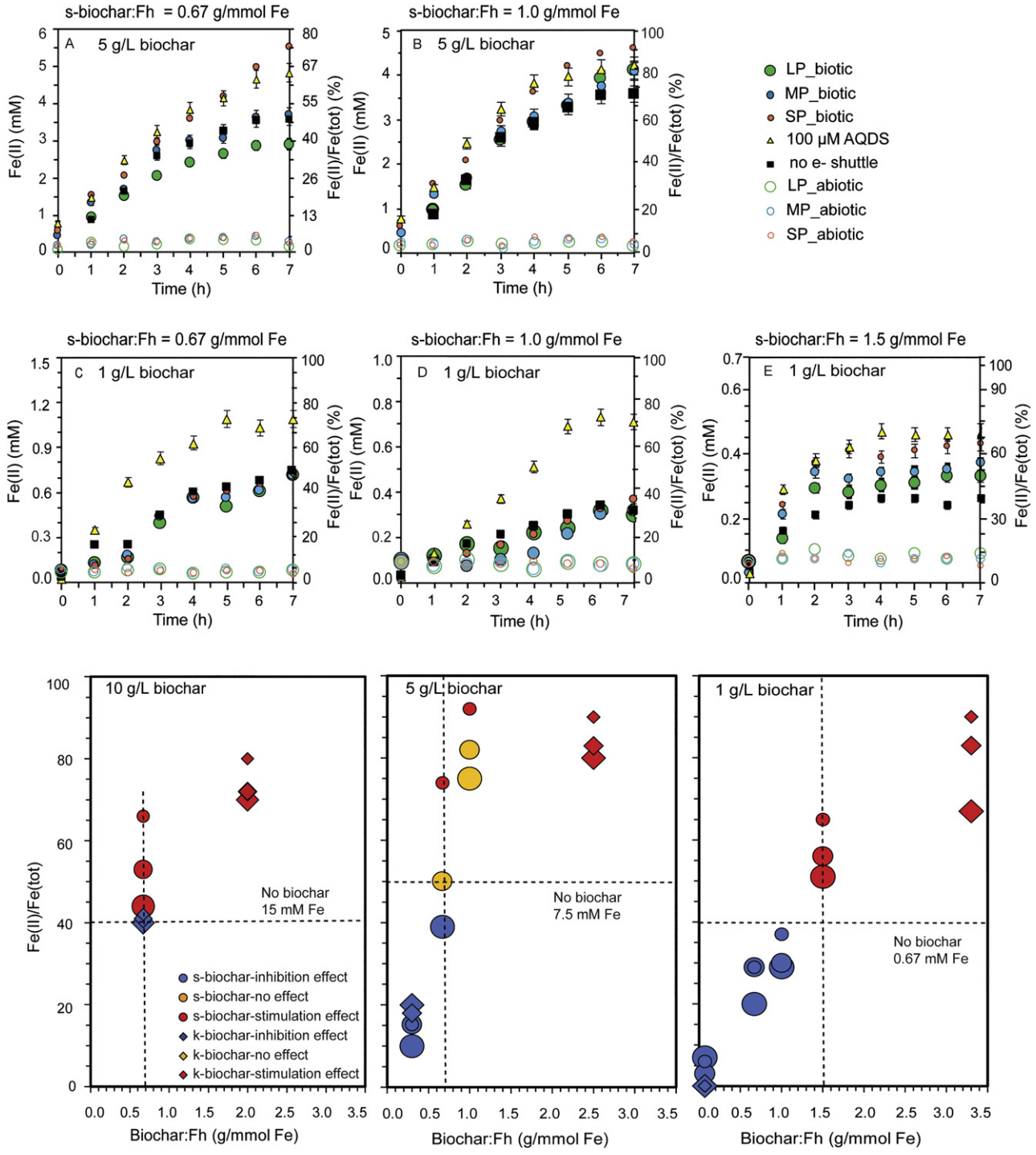

Fig. 2. Top: Microbial ferrihydrite (Fh) reduction by *S. oneidensis* MR-1 at different Swiss biochar (s-biochar) particle sizes and biochar:Fh ratios (g biochar per mmol Fe). (A) Ratio 0.67 with 7.5 mM Fh and 5 g/L biochar; (B) Ratio 1.0 with 5 mM Fh and 5 g/L s-biochar; (C) Ratio 0.67 with 1.5 mM Fh and 1 g/L s-biochar; (D) Ratio 1.0 with 1 mM Fh and 1 g/L s-biochar; (E) Ratio 1.5 with 0.67 mM Fh and 1 g/L s-biochar. Error bars represent standard deviations of triplicate experimental setups. The results for 16-h incubations are shown in Fig. S6. Bottom: Influence of biochar (s-biochar and KonTiki biochar, k-biochar) particle size (indicated by the size of the symbols) and biochar:Fh ratios (g biochar per mmol Fe) on microbial Fh reduction. Blue symbols and red symbols show experiments in which inhibition (blue) and stimulation (red) of microbial Fh reduction were observed, while yellow symbols show experiments where biochar addition had no effect on rates of Fe(III) reduction compared to setups without biochar addition.

conducted with higher cell numbers (5×10^9 cells/mL) at the same s-biochar/Fh ratio of 0.3 g/mmol Fe showed no apparent increase in rates and extent of Fh reduction (Fig. S13), suggesting that there were still not enough cells that had access to Fh - either directly or indirectly via redox-active s-biochar particles.

Influence of Cell-Biochar-Ferrihydrite Aggregation (Depending on Biochar Particle Size and Biochar:Fh Ratio) on Electron Transfer Mechanisms and the Fate of Electrons from Lactate Oxidation. To evaluate the electron transfer mechanisms and the fate of electrons released from lactate oxidation in the presence of different biochar:Fh ratios, we calculated the percentage of electrons recovered as Fe(II), electrons theoretically accepted by functional groups of biochar and remaining electrons in biochar carbon matrices or in cells (Table S2, Fig. 4). This allows to evaluate the contributions of different electron transfer pathways, i.e.

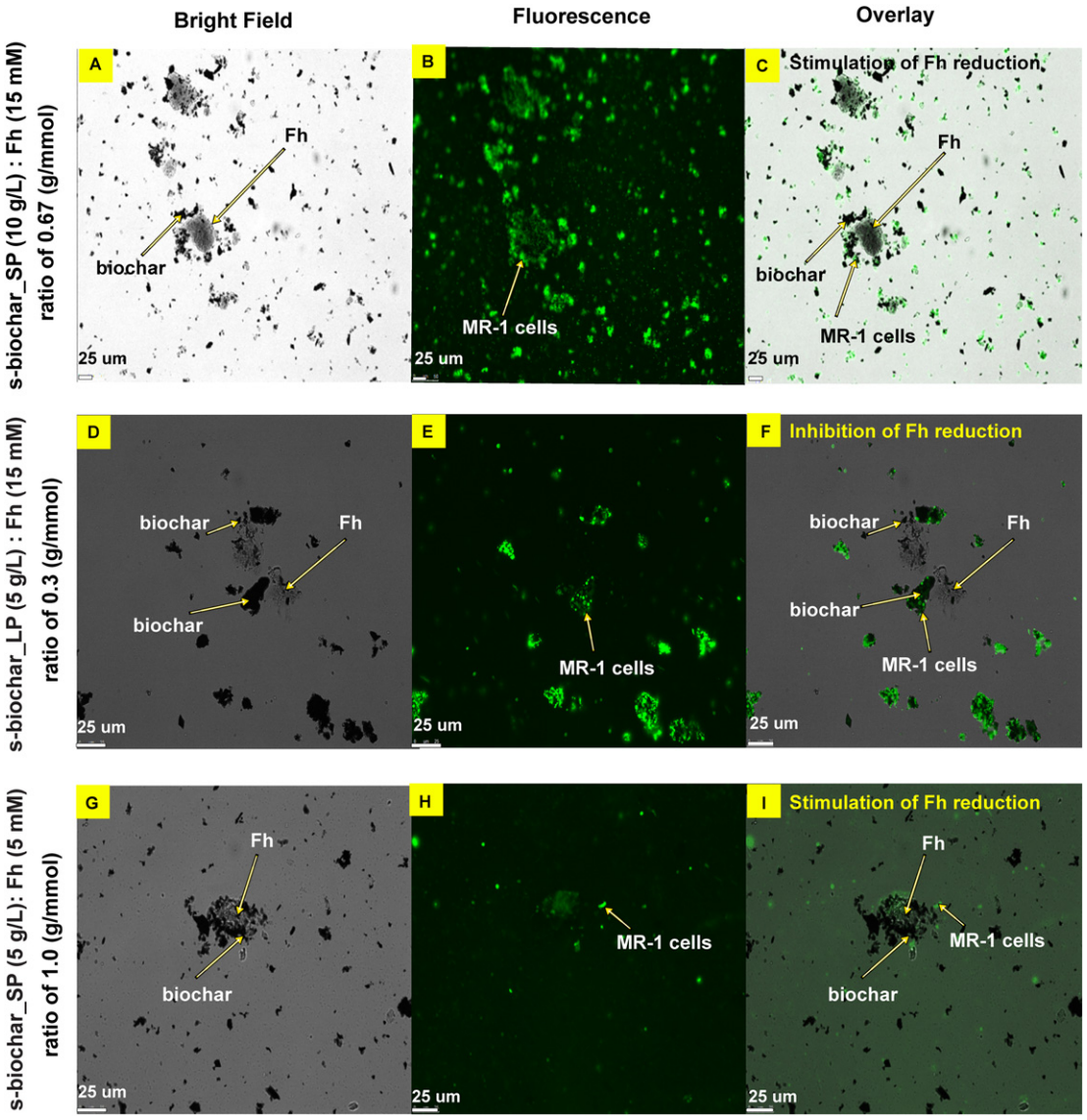

Fig. 3. Aggregation of Swiss biochar (s-biochar) with ferrihydrite (Fh) and *S. oneidensis* MR-1 cells (stained by DNA dye Syto 9 combined with propidium iodide) analyzed by fluorescence microscopy. Experiments with s-biochar:Fh ratios (g/mmol) of 0.67 (A-C), 0.3 (D-F) and 1.0 (G-I). The gray parts represent Fh, the black parts represent s-biochar particles and MR-1 cells are shown in green. (A) 10 g/L small particle size (SP) s-biochar associated with 15 mM Fh (bright field, no fluorescence), (B) MR-1 cells attached to particles (fluorescence), and (C) overlay of A and B showing the aggregation of MR-1 cells with s-biochar and Fh (which showed a stimulation of microbial Fh reduction). (D) 5 g/L large particle size (LP) s-biochar and 15 mM Fh, (E) MR-1 cells and particles, and (F) overlay of D and E showing aggregation of MR-1 cells with s-biochar and Fh (which showed an inhibition of microbial Fh reduction). (G) 5 g/L SP s-biochar associated with 5 mM Fh, (H) MR-1 cells attached to particles and (I) overlay of G and H showing the aggregation of MR-1 cells with s-biochar and Fh where a stimulation of microbial Fh reduction was observed again. Please note that the fluorescence images shown are representative images chosen among ca. 100 images. Due to overlay of cells, minerals and s-biochar particles they cannot be used for quantification of certain aggregates/associations.

electron transfer via redox cycling of functional groups of biochar as well as conductance and capacitance of the biochar carbon matrices, based on the extent of aggregation of cells, biochar and Fh (Fig. 5).

In the presence of biochar and Fh (biochar:Fh ratio of 0.067 g/mmol Fe), for all particle sizes, 10–11% of the electrons that were released from lactate oxidation by *S. oneidensis* MR-1 to acetate and CO_2 (4 electrons per lactate) were recovered as Fe(II) and up to 8–9% of the released electrons could have been (theoretically) accepted by the redox-active functional groups of the biochar. Up to 80% of the remaining electrons were probably stored either within the biochar due to its electrical double-layer capacitance or in the cells (Figs. 4 and 5). In experiments with a biochar to Fh ratio of 0.067, biochar was poorly associated with Fh (i.e. the extent of aggregation of biochar with Fh is close to 0%; see Fig. S14a). The electrons donated from MR-1 cells were therefore stored in the π-electron system of the carbon matrices instead of being released to Fh. These stored electrons were surrounded and charge balanced most likely by protons which were co-products with electrons in the MR-1 metabolism (Pinchuk et al., 2011). This microbial electron-proton system could have constituted an electrical double-layer in biochar and was responsible for capacitive electron storage. A similar electron storage mechanism has also been found in capacitive microbial fuel cells (Deeke et al., 2012). Due to the insufficient association of biochar and Fh, the 10–11% of Fe(II) formation probably stemmed from cells that were directly attached to Fh and reduced the Fh.

When increasing the biochar:Fh ratio to 0.3 g/mmol Fe with 5 g/L of biochar, more electrons were recovered as Fe(II) (13–22%) and more electrons can be accepted by redox-active functional groups of the biochar (34–36%). The fraction of remaining electrons, probably stored by the capacitance of the carbon matrices, decreased to 42–53%. When further increasing the biochar/Fh ratio to 0.67 g/mmol Fe, although a similar percentage of electrons can be accepted by the functional groups of

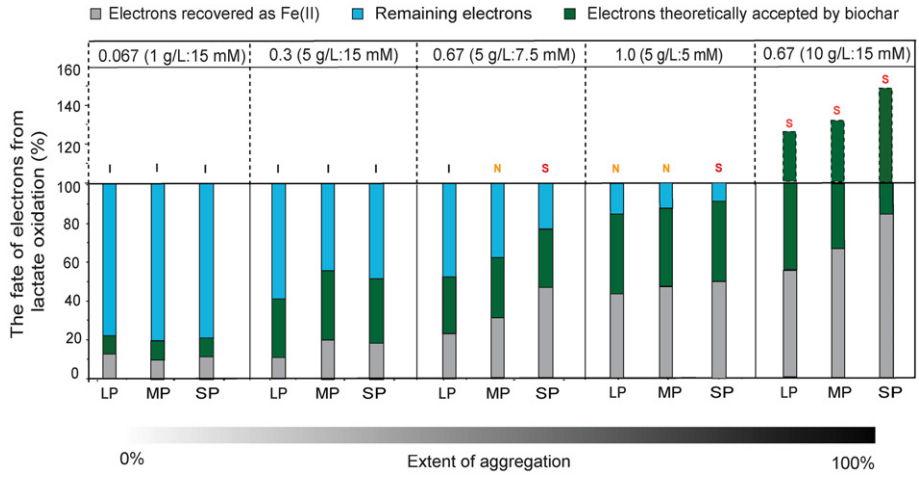

Fig. 4. The fate of electrons released from lactate oxidation in the presence of large (LP), medium (MP) and small particles (SP) of Swiss biochar (s-biochar) at biochar:Fh ratios (g biochar/mmol Fe) of 0.067, 0.3, 0.67 and 1.0. Electrons released from oxidation of lactate to acetate are recovered as either i) Fe(II) stemming from microbial Fe(III) reduction ((quantified as Fe(II) in our experiments), ii) electrons theoretically accepted by s-biochar (quantified from EAC of biochar measured) or iii) remaining electrons calculated as the difference between electrons released from lactate oxidation and electrons accepted by s-biochar and recovered as Fe(II), which includes electrons stored by the carbon matrices capacitance and electrons stored in cells (e.g. as lactate). 'I' (black), 'N' (orange), and 'S' (red) symbols on the top of bars indicate whether inhibition, no change or stimulation of microbial Fe(III) reduction occurred compared to setups without biochar amendment.

biochar as in the 0.3 ratio setup, more electrons were recovered as Fe(II) (26–48%) and consequently less electrons (19–39%) were stored in the biochar and/or cells. These results suggest that at higher biochar/Fh ratios, as a result of the increased aggregation of biochar with Fh, electrons were directly transferred from the cells to the Fh by the conductive biochar carbon matrices, promoting Fe(II) formation, (Fig. S14b);

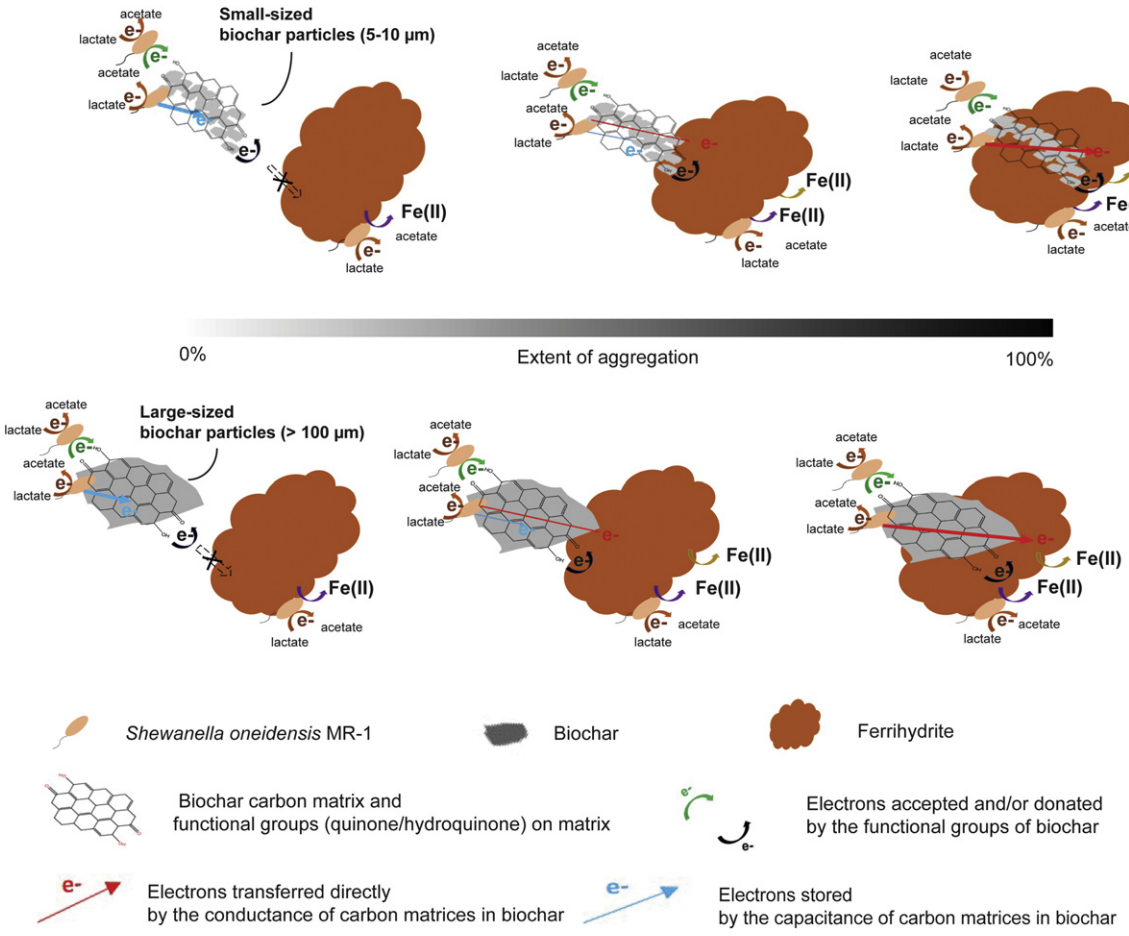

Fig. 5. Electron transfer pathways between *S. oneidensis* MR-1 cells and ferrihydrite (Fh) in the presence of small-sized (2–10 μm) and large-sized biochar particles (>100 μm) depending on the extent of aggregation of biochar and Fh. When Fh as electron acceptor is not close to the biochar (i.e. the extent of aggregation of biochar to Fh is close to 0%), electrons released from microbial lactate oxidation can be accepted by the quinone groups of biochar or can be stored in biochar by the electrical double-layer capacitance of the carbon matrices. In this case, Fh reduction is only possible by cells directly associated with the Fh. With increasing extent of aggregation of biochar with Fh, the electrons start to be transferred to Fh by both electron donation of the hydroquinone groups and direct electron transfer by the electrical conductance of the carbon matrices, so that more and more Fe(II) will be produced.

the biochar conductivity was similar as it was described for a 700 °C pyrolyzed sawdust biochar which contributed to electron transfer during persulfate oxidation (He et al., 2019). At the same biochar/Fh ratio of 0.67 g/mmol Fe with small-sized particles or at an even higher biochar/Fh ratio of 1.0 g/mmol Fe with all particle sizes, only a small fraction of electrons (8–19%) was stored in biochar and cells (Fig. 4) suggesting an efficient transfer of electrons from the cells to the Fh via the conductive biochar and via reduced functional groups of biochar. Generally, small-sized particles showed higher rates of Fe(II) formation and higher percentages of electrons recovered as Fe(II) than medium- and large-sized biochar particles probably because smaller biochar particles show a higher extent of aggregation with Fh (see e.g. Fig. S14c) facilitating direct electron transfer to Fh.

In setups with a biochar/Fh ratio of 0.67 g/mmol and 10 g/L biochar, for the three particle sizes (SP, MP, LP) up to 56–85% of electrons were recovered as Fe(II) and 65–67% could have been theoretically accepted by the functional groups of biochar, respectively (Fig. 4, Fig. S14d), leading in all cases to a stimulation of Fe(II) formation compared to the biochar-free setups. Due to the intimate contact of the biochar with the Fh, in these cases probably no electrons were stored in the carbon matrices, i.e. most electrons were transferred from biochar to Fh (Fig. 4). It is obvious from these experiments that the stimulation of Fh reduction by biochar required a certain biochar/Fh ratio to facilitate direct electron transfer from bacteria via biochar to Fh (Fig. 5).

3.4. Potential factors influencing the aggregation of cells, biochar and Fh

To better understand the aggregation of cells with biochar and Fh, we determined the zeta potential of the SP, MP and LP s-biochar. SP-sized s-biochar showed a more negative potential (−26.5 ± 0.3 mV) than MP-sized (−22.8 ± 0.1 mV) and LP-sized biochar (−15.2 ± 0.2 mV) (Fig. S14). These results are in agreement with previous studies (Eusterhues et al., 2014) on oak-derived biochar pyrolyzed at 650 °C (particles of 0.25–2 mm) with a zeta potential close to −10 mV. The zeta potentials of the s-biochar particles were more negative than those of the MR-1 cells (−7.65 ± 0.3 mV; similar as other values of −6.4 mV) (Wu et al., 2017), suggesting that in particular the SP-sized s-biochar, that showed the most negative value, is expected to attach to a larger extent to the positively charged Fh with +18 mV (Li et al., 2015) than the cells (Fig. 3A, D and G). Consequently, a fast electron transfer from cells via biochar can happen when cells are attached to biochar.

We also observed that MR-1 cells were attached more to the negatively-charged biochar particles than to the Fh particles (Fig. 3F), suggesting that bacteria can bind efficiently to the biochar surface using hydrophobic interactions thus overcoming the repulsion by the negative surface charges (Suliman et al., 2017). Alternatively, the interactions of the negatively charged cells and the negatively charged biochar maybe supported by bridging cations. Additionally, with increasing Fh concentrations, the mineral particles can aggregate forming large mineral assemblages with a lower weight-based surface area (Villacís-García et al., 2015; Bompoti et al., 2017; Hiemstra and Van Riemsdijk, 2009) and less binding sites for biochar and cells. A recent study observed an inhibition of Fh reduction by *S. oneidensis* MR-1 by graphene material (Liu et al., 2018) and explained this by a limited accessibility of the Fh by the microorganisms. Our and their findings together indicate that on the one hand certain ratios of solid electron shuttle to Fh (in our case biochar/Fh) and a close aggregation of the biochar, MR-1 cells, and Fh is required to stimulate microbial Fh reduction and on the other hand high amounts of graphene-based materials or biochar present can inhibit electron transfer. Three-dimensional analysis of the same samples using CLSM confirmed the observations from fluorescence microscopy regarding cell-mineral-biochar aggregations and also revealed the secretion of extracellular polymeric substances (EPS) (Fig. S16). EPS can help microorganisms to attach to minerals and facilitate electron transfer between cells and the solid surface (Harris et al., 2010) owing to its redox properties (Cao et al., 2011; Li et al., 2016). Therefore, we investigated whether biochar influenced EPS secretion from MR-1 by quantification of the protein and polysaccharide contents after addition of different concentrations of s-biochar and 15 mM Fh (Fig. S17). We observed that low concentrations (1 and 5 g/L) of SP s-biochar decreased the protein but increased the polysaccharide content in EPS compared to setups without electron shuttle, while higher concentrations (10 g/L) of SP s-biochar and AQDS (100 μM) behaved similar as setups without electron shuttle and showed a slight increase in protein contents compared to low concentration biochar amendments. Based on these observations, it is conceivable that biochar addition influenced the concentrations of redox-active compounds within the EPS and that these differences influence electron transport from the outer membrane of MR-1 cells via EPS to biochar particles. EPS was indeed shown to store redox-active flavins and cytochromes, enabling EPS-bound cells to transport electrons extracellularly to electron acceptors via extracellular electron transfer (EET), i.e. electron hopping across the EPS (Xiao et al., 2017). Additionally, a previous study (Caccavo, 1999) suggested the contribution of surface proteins to the adhesion of the dissimilatory Fe(III)-reducing bacterium *S. alga* BrY to poorly crystalline ferric hydroxide. The presence of lower and higher concentrations of potentially redox-active proteins in the EPS may offer additional explanations how low biochar concentrations (1 and 5 g/L) can inhibit and high concentrations (10 g/L) can stimulate electron transfer between *S. oneidensis* MR-1 and Fh.

3.5. Environmental implications

Compared to previous studies that showed how biochar concentrations influence microbial ferrihydrite reduction, our present study revealed that stimulation or inhibition of microbial Fe(III) reduction depends on the aggregation of bacteria and biochar with the Fh influenced by biochar particle size and biochar/Fh ratio. These findings allow better evaluating the impact of biochar on electron transfer processes in soils or sediments. Biochar addition was shown to mobilize arsenic in paddy soils due to enhanced dissimilatory Fe(III) reduction (Wang et al., 2017a, 2017b), which is possibly attributed to the presence of high biochar/Fe(III) minerals with close aggregation of biochar, cells and minerals. In agricultural soils, biochar favored microbial Fe(III) reduction and thus lowered greenhouse gas emission (i.e. N_2O and CH_4) (Wang et al., 2017a, 2017b). Microbial Fe(III) mineral reduction and methanogenesis compete for the same electron donors, in particular in anoxic environments such as paddy soils or wetlands (Achtnich et al., 1995; Chidthaisong and Conrad, 2000; Teh et al., 2008). Based on our study, it is evident that it has also to be determined how much biochar of which particle size needs to be added to paddy soil to favor or inhibit microbial Fe(III) reduction therefore controlling methane emission.

Biochar addition to soils could alter the identity of secondary iron minerals formed during Fe(III) reduction and due to differences in mineral solubility, particle size and surface area, this could impact the fate of toxic metals as well as nutrients (Borch et al., 2010). Such effects on environmental processes are expected not only to happen after addition of biochar, but also in environments that have significant concentrations of pyrogenic carbon, such as soils (Schmidt and Noack, 2000; Lehmann et al., 2009), sediments (Beesley et al., 2001), and aqueous marine and terrestrial habitats (Bird et al., 2015; Jung et al., 2016). The μm- and nm-particles of biochar as we have investigated here in the present study represent very reactive fractions participating in Earth's carbon cycling and various biogeochemical processes due to their reactivity and high mobility functioning as a carrier and thus facilitating the transport of contaminants and phosphorus transport alkaline soils (Chen et al., 2017; Chen et al., 2018; Wang et al., 2013). Aggregation of biochar and cells with Fe(III) mineral impacts electron transfer via biochar, which may further influence the environmental association,

transport, retention and fate of containments, organic matter and metals.

Declaration of competing interest

The authors declare that they have no known competing financial interests or personal relationships that could have appeared to influence the work reported in this paper.

Acknowledgements

We gratefully acknowledge support by the China Scholarship Council Foundation (No. 201606510018) and we also thank Ellen Röhm for particle size and TOC/DOC analysis and help with *S. oneidensis* cultivation. We also thank Annette Flicker for FTIR analysis.

Appendix A. Supplementary data

The Supporting Information is available free of charge on the xxx Publications website at DOI:https://doi.org/10.1016/j.scitotenv.2019.135515. It contains data on redox properties and functional groups of biochars, detailed experimental procedures and calculations, and information on three-dimensional aggregates and secondary mineral analysis.

References

Achtnich, C., Bak, F., Conrad, R., 1995. Competition for electron-donors among nitrate reducers, ferric iron reducers, sulfate reducers, and methanogens in anoxic paddy soil. Biol. Fertil. Soil. 19 (1), 65–72. https://doi.org/10.1007/BF00336349.

Amstaetter, K., Borch, T., Kappler, A., 2012. Influence of humic acid imposed changes of ferrihydrite aggregation on microbial Fe(III) reduction. Geochim. Cosmochim. Acta 85, 326–341. https://doi.org/10.1016/j.gca.2012.02.003.

Bauer, I., Kappler, A., 2009. Rates and extent of reduction of Fe(III) compounds and O_2 by humic substances. Environ. Sci. & Technol. 43 (13), 4902–4908. https://doi.org/10.1021/es900179s.

Beesley, L., Moreno-Jiménez, E., Gomez-Eyles, J.L., Harris, E., Robinson, B., Sizmur, T., 2001. A review of biochars' potential role in the remediation, revegetation and restoration of contaminated soils. Environ. Pollut. 159 (12), 3269–3282.

Benner, S., Hansel, C., Wielinga, B., M Barber, T., Fendorf, S., 2002. Reductive dissolution and biomineralization of iron hydroxide under dynamic flow conditions. Environ. Sci. & Technol. 36 (8), 1705–1711. https://doi.org/10.1021/es0156441.

Bird, M.I., Wynn, J.G., Saiz, G., Wurster, C.M., McBeath, A., 2015. The pyrogenic carbon cycle. Annu. Rev. Earth Planet. Sci. 43, 273–298.

Bompoti, N., Chrysochoou, M., Machesky, M., 2017. Surface structure of ferrihydrite: insights from modeling surface charge. Chemi. Geol 464, 34–45.

Borch, T., Kretzschmar, R., Kappler, A., Van Cappellen, P., Ginder-Vogel, M., Voegelin, A., Campbell, K., 2010. Biogeochemical redox processes and their impact on contaminant dynamics. Environ. Sci. & Technol. 44 (1), 15–23. https://doi.org/10.1021/es9026248.

Byrne, J.M., Van der Laan, G., Figueroa, A.I., Qafoku, O., Wang, C., Pearce, C.I., Jackson, M., Feinberg, J., Rosso, K.M., Kappler, A., 2016. Size dependent microbial oxidation and reduction of magnetite nano- and micro-particles. Sci. Rep. 6, 30969. https://doi.org/10.1038/srep30969.

Caccavo, F., 1999. Protein-mediated adhesion of the dissimilatory Fe (III)-reducing bacterium *Shewanella alga BrY* to hydrous ferric oxide. App. Environ. Microbiol. 65 (11), 5017–5022.

Cao, B., Ahmed, B., Kennedy, D.W., Wang, Z., Shi, L., Marshall, M.J., Fredrickson, J.K., Isern, N.G., Majors, P.D., Beyenal, H., 2011. Contribution of extracellular polymeric substances from *Shewanella sp. HRCR-1* biofilms to U(VI) immobilization. Environ. Sci. & Technol. 45 (13), 5483–5490. https://doi.org/10.1021/es200096j.

Cayuela, M.L., Sánchez-Monedero, M., Roig, A., Hanley, K., Enders, A., Lehmann, J., 2013. Biochar and denitrification in soils: when, how much and why does biochar reduce N_2O emissions? Sci. Rep. 3, 1723. https://doi.org/10.1038/srep017312.

Chen, M., Wang, D.J., Yang, F., Xu, N., Cao, X.D., 2017. Transport and retention of biochar nanoparticles in a paddy soil under environmentally-relevant solution chemistry conditions. Environ. Pollut. 230, 540–549.

Chen, M., Alim, N., Zhang, Y., Xu, N., Cao, X., 2018. Contrasting effects of biochar nanoparticles on the retention and transport of phosphorus in acidic and alkaline soils. Environ. Pollut. 239, 562–570. https://doi.org/10.1016/j.envpol.2018.04.050.

Chidthaisong, A., Conrad, R., 2000. Turnover of glucose and acetate coupled to reduction of nitrate, ferric iron and sulfate and to methanogenesis in anoxic rice field soil. FEMS Microbiol. Ecol. 31 (1), 73–86.

Deeke, A., Sleutels, T.H., Hamelers, H.V., Buisman, C.J., 2012. Capacitive bioanodes enable renewable energy storage in microbial fuel cells. Environ. Sci. Technol. 46 (6), 3554–3560.

Deluca, T., Gundale, M.J., Mackenzie, M.D., Jones, D., 2009. Biochar Effects on Soil Nutrient Transformations. Earthscan Publications Ltd.

Eusterhues, K., Hädrich, A., Neidhardt, J., Küsel, K., Keller, T., Jandt, K.D., Totsche, K., 2014. Reduction of ferrihydrite with adsorbed and coprecipitated organic matter: microbial reduction by *Geobacter bremensis* vs. abiotic reduction by Na-dithionite. Biogeosci. 11 (4), 11. https://doi.org/10.5194/bgd-11-6039-2014.

Frølund, B., Palmgren, R., Keiding, K., Nielsen, P.H., 1996. Extraction of extracellular polymers from activated sludge using a cation exchange resin. Water Res. 30 (8), 1749–1758. https://doi.org/10.1016/0043-1354(95)00323-1.

Fuller, S.J., McMillan, D.G.G., Renz, M.B., Schmidt, M., Burke, I.T., Stewart, D.I., 2014. Extracellular electron transport-mediated Fe(III) reduction by a community of alkaliphilic bacteria that use flavins as electron shuttles. Appl. Environ. Microbiol. 80 (1), 128–137. https://doi.org/10.1128/AEM.02282-13.

Gescher, J., Kappler, A., 2013. Microbial Metal Respiration: From Geochemistry to Potential Applications. Springer Heidelberg Press, New York, Dordrecht, London.

Glasser, R.N., Saunders, H.S., Newman, K.D., 2017. The colorful world of extracellular electron shuttles. Annu. Rev. Microbiol. 71, 731–751. https://doi.org/10.1146/annurev.micro-090816-093919.

Gouveia, S.E.M., Pessenda, L.C.R., 2000. Datation parte 14C de charbons inclus dans le sol por l'etude du role de la remontee biologique de matière et du colluvionnement dans la formation de latosols de l'etat de Sao Paulo, Bresil. C.R. Acad.Sci. 330, 133–138.

Gul, S., Whalen, J., 2016. Biochemical cycling of nitrogen and phosphorus in biochar-amended soils. Soil Biol. Biochem. 103, 1–15. https://doi.org/10.1016/j.soilbio.2016.08.001.

Hagemann, N., Kammann, C.I., Schmidt, H.-P., Kappler, A., Behrens, S., 2017. Nitrate capture and slow release in biochar amended compost and soil. PLoS One 12 (2), 171–214. https://doi.org/10.1371/journal.pone.0171214.

Harris, H.W., El-Naggar, M.Y., Bretschger, O., Ward, M.J., Romine, M.F., Obraztsova, A.Y., Nealson, K.H., 2010. Electrokinesis is a microbial behavior that requires extracellular electron transport. Natl. Acad. Sci. U.S.A.. 107 (1), 326–331.

Harter, J., Krause, H.M., Schuettler, S., Ruser, R., Fromme, M., Scholten, T., Kappler, A., Behrens, S., 2014. Linking N_2O emissions from biochar-amended soil to the structure and function of the N-cycling microbial community. Isme. J. 8 (3), 660–674. https://doi.org/10.1038/ismej2013.160.28.

He, J., Xiao, Y., Tang, J., Chen, H., Sun, H., 2019. Persulfate activation with sawdust biochar in aqueous solution by enhanced electron donor-transfer effect. Sci. Total Environ. 690, 768–777.

Hiemstra, T., Van Riemsdijk, W.H., 2009. A surface structural model for ferrihydrite I: sites related to primary charge, molar mass, and mass density. Geochim. Cosmochim. Acta 73 (15), 4423–4436.

Ji, H., Zhao, X., Qiao, Z., Jung, J., Zhu, Y., Lu, Y., Ruoff, R.S., 2014. Capacitance of carbon-based electrical double-layer capacitors. Nat. Commun. 5, 3317.

Jiang, J., Kappler, A., 2008. Kinetics of microbial and chemical reduction of humic substances: implications for electron shuttling. Environ. Sci. & Technol. 42 (10), 3563–3569. https://doi.org/10.1021/es7023803.

Jung, K.W., Kim, K., Jeong, T.U., Ahn, K.H., 2016. Influence of pyrolysis temperature on characteristics and phosphate adsorption capability of biochar derived from waste-marine macroalgae (Undaria pinnatifida roots). Bioresour. Technol. 200, 1024–1028.

Kappler, A., Straub, K.L., 2005. Geomicrobiological cycling of iron. Rev. Mineral. Geochem. 59, 85–108. https://doi.org/10.2138/rmg.

Kappler, A., Wuestner, M.L., Ruecker, A., Harter, J., Halama, M., Behrens, S., 2014. Biochar as an electron shuttle between bacteria and Fe(III) minerals. Environ. Sci. & Technol. Lett. 1 (8), 339–344. https://doi.org/10.1021/ez5002209.005.59.5.

Keiluweit, M., Nico, P.S., Johnson, M.G., Kleber, M., 2010. Dynamic molecular structure of plant biomass-derived black carbon (biochar). Environ. Sci. Technol. 44, 1247–1253.

Klüpfel, L., Keiluweit, M., Kleber, M., Sander, M., 2014. Redox properties of plant biomass-derived black carbon (biochar). Environ. Sci. & Technol. 48 (10), 5601–5611. https://doi.org/10.1021/es500906d.

Konhauser, K., Kappler, A., Roden, E.E., 2011. Iron in microbial metabolisms. Elements 7 (2), 89–93. https://doi.org/10.2113/gselments.7.2.8.9.

Lehmann, J., Joseph, S., 2015. Biochar for Environment Management Science and Technology (London. Sterling, VA).

Lehmann, J., Czimczik, C., Laird, D., Sohi, S., 2009. Stability of biochar in soil. Biochar for Environmental Management: Science and Technology. Earthscan in the UK and USA, pp. 183–206.

Li, F., Geng, D., Cao, Q., 2015. Adsorption of As (V) on aluminum-, iron-, and manganese-(oxyhydr) oxides: equilibrium and kinetics. Desalin. Water Treat. 56 (7), 1829–1838.

Li, S.W., Sheng, G.P., Cheng, Y.-Y., Yu, H.Q., 2016. Redox properties of extracellular polymeric substances (EPS) from electroactive bacteria. Sci. Rep. 6, 39098. https://doi.org/10.1038/srep39098.

Liu, G., Yu, H., Wang, N., Jin, R., Wang, J., Zhou, J., 2018. Microbial reduction of ferrihydrite in the presence of reduced graphene oxide materials: alteration of Fe(III) reduction rate, biomineralization product and settling behavior. Chemi. Geol. 476, 272–279. https://doi.org/10.1016/j.chemgeo.2017.11.023.

Lovley, D.R., Coates, J.D., BluntHarris, E.L., Phillips, E.J.P., Woodward, J.C., 1996. Humic substances as electron acceptors for microbial respiration. Nature 382 (6590), 445–448. https://doi.org/10.1038/382445a0.

Lovley, D.R., Holmes, D.E., Nevin, K.P., 2004. Dissimilatory Fe(III) and Mn(IV) reduction. Adv. Microb. Physiol. 49, 219–286. https://doi.org/10.1016/S006S-2911(04)49005-5.

Malvankar, N.S., Lovley, D.R., 2014. Microbial nanowires for bioenergy applications. Curr. Opin. Biotechnol. 27, 88–95. https://doi.org/10.1016/j.copbio.2013.12.003.

Marsili, E., Baron, B.D., Shikhare, D.I., Coursolle, D., Gralnick, A.J., Bond, R.D., 2008. *Shewanella* secretes flavins that mediate extracellular electron transfer. Proc. Natl. Acad. Sci. U. S. A. 105 (10), 3968–3973. https://doi.org/10.1073/pnas.0710525105.

Myers, C., Myers, J., 2003. Cell surface exposure of the outer membrane cytochromes of *Shewanella oneidensis* MR-1. Lett. Appl. Microbiol. 37 (3), 254–258. https://doi.org/10.1046/j.1472-765X.2003.01389.x.

Newman, K.D., 2005. Direct and indirect mechanisms of microbial iron reduction. Geochim. Cosmochim. Acta 4 (1), 5520–5525.
Nguyen, B.T., Lehmann, J., Kinyangi, J., Smernik, R., Riha, S.J., Engelhard, M.H., 2008. Long-term black carbon dynamics in cultivated soil. Biogeochemistry 89 (3), 295–308.
O'Loughlin, E.J., 2008. Effects of electron transfer mediators on the biodegradation of lepidocrocite (γ-FeOOH) by *Shewanella putrefaciens* CN32. Environ. Sci. Technol. 42 (18), 6876–6882. https://doi.org/10.1021/es800686d.
Pinchuk, G.E., Geydebrekht, O.V., Hill, E.A., Reed, J.L., Konopka, A.E., Beliaev, A.S., Fredrickson, J.K., 2011. Pyruvate and lactate metabolism by Shewanella oneidensis MR-1 under fermentation, oxygen limitation, and fumarate respiration conditions. Appl. Environ. Microbiol. 77 (23), 8234–8240.
Rau, J., Knackmuss, H.-J., Stolz, A., 2002. Effects of different quinoid redox mediators on the anaerobic reduction of azo dyes by bacteria. Environ. Sci. Technol. 36 (7), 1497–1504. https://doi.org/10.1021/es010227.
Reguera, G., McCarthy, D.K., Mehta, T., Nicoll, S.J., Tuominen, M., Lovley, R.D., 2005. Extracellular electron transfer via microbial nanowires. Nature 435 (7045), 1098–10101. https://doi.org/10.1038/nature03661.
Roden, E.E., Kappler, A., Bauer, I., Jiang, J., Paul, A., Stoesser, R., Konishi, H., Xu, H., 2010. Extracellular electron transfer through microbial reduction of solid-phase humic substances. Nature Geo 3, 417–421. https://doi.org/10.1038/ngeo870.21.
Schmidt, M.W., Noack, A.G., 2000. Black carbon in soils and sediments: analysis, distribution, implications, and current challenges. Global Biogeochemical. Cy. 14 (3), 777–793.
Scott, D.T., McKnight, D.M., Blunt-Harris, E.L., Kolesar, S.E., Lovley, D.R., 1998. Quinone moieties act as electron acceptors in the reduction of humic substances by humics-reducing microorganisms. Environ. Sci. Technol. 32 (19), 2984–2989. https://doi.org/10.1021/es982014z.
Shi, L., Rosso, K.M., Zachara, J.M., Fredrickson, J.K., 2012. Mtr extracellular electron-transfer pathways in Fe(III)-reducing or Fe(II)-oxidizing bacteria: a genomic perspective. Biochem. Soc. Trans. 40 (6), 1261–1267. https://doi.org/10.1042/BST20120098.
Shi, L., Dong, H., Reguera, G., Beyenal, H., Lu, A., Liu, J., Yu, H.-Q., Fredrickson, J.K., 2016. Extracellular electron transfer mechanisms between microorganisms and minerals. Nat. Rev. Microbiol. 14 (10), 651–662. https://doi.org/10.1038/nrmicro.2016.93.
Song, B., Chen, M., Zhao, L., Qiu, H., Cao, X., 2019. Physicochemical properties and colloidal stability of micro- and nano particle biochar derived from a verity of feedstock sources. Sci. Tot. Environ. 15 (661), 685–695. https://doi.org/10.1016/j.scitotenv.2019.01.193.
Stookey, L.L., 1970. Ferrozine—A new spectrophotometric reagent for iron. Anal. Chem. 42 (7), 779–781. https://doi.org/10.1021/ac60289a016.
Sudirjo, E., Strik, D., Buisman, C.J., 2019. Marine sediment mixed with activated carbon allows electricity production and storage from internal and external energy sources: a new rechargeable bio-battery with bi-directional electron transfer properties. Front. Microbiol. 10, 934.
Suliman, W., Harsh, J.B., Fortuna, A.M., Garcia-Pérez, M., Abu-Lail, N.I., 2017. Quantitative effects of biochar oxidation and pyrolysis temperature on the transport of pathogenic and nonpathogenic Escherichia coli in biochar-amended sand columns. Environ. Sci. Technol. 51 (9), 5071–5081.
Sun, T., Levin, B.D.A., Guzman, J.J.L., Enders, A., Muller, D.A., Angenent, L.T., Lehmann, J., 2017. Rapid electron transfer by the carbon matrix in natural pyrogenic carbon. Nat. Commun. 8, 14873.
Sun, T., Levin, B.D.A., Schmidt, M.P., Guzman, J.J.L., Enders, A., Martínez, C.E., Muller, D.A., Angenent, L.T., Lehmann, J., 2018. Simultaneous quantification of electron transfer by carbon matrices and functional groups in pyrogenic carbon. Environ. Sci. Technol. 52 (15), 8538–8547. https://doi.org/10.1021/acs.est.8bb02340.
Teh, Y.A., Dubinsky, E.A., Silver, W.L., Carlson, C.M., 2008. Suppression of methanogenesis by dissimilatory Fe(III)-reducing bacteria in tropical rain forest soils: implications for ecosystem methane flux. Glob. Change Biol. 14 (2), 413–422. https://doi.org/10.1111/j.1365-2486.2007.01487x.
Villacís-García, M., Ugalde-Arzate, M., Vaca, K., Escobar, M., Martínez-Villegas, M., 2015. Laboratory synthesis of goethite and ferrihydrite of controlled particle sizes. Bol. Soc. Geol. Mex. 67 (3), 433–446.
Wang, D.J., Zhang, W., Hao, X.Z., Zhou, D.M., 2013. Transport of biochar in saturated granular media: effects of pyrolysis temperature and particle size. Environ. Sci. Technol. 47 (2), 821–828 41. 10.1021.es303794d.
Wang, N., Chang, Z.Z., Xue, X.M., Yu, J.G., Shi, X.X., Ma, L.Q., Li, H.B., 2017a. Biochar decreases nitrogen oxide and enhances methane emissions via altering microbial community composition of anaerobic paddy soil. Sci. Total Environ. 581, 689–696.
Wang, N., Xue, X.M., Juhasz, A.L., Chang, Z.Z., Li, H.B., 2017b. Biochar increases arsenic release from an anaerobic paddy soil due to enhanced microbial reduction of iron and arsenic. Environ. Pollut. 220, 514–522.
Weber, K., Achenbach, A.L., Coates, D.J., 2006. Microbes pumping iron: anaerobic microbial iron oxidation and reduction. Nat. Rev. Microbiol. 4 (10), 752–764 Biochar decreases nitrogen oxide and enhances methane emissions via altering microbial community composition of anaerobic paddy soil. https://doi.org/10.1038/nrmicro1490.
Weber, F.-A., Voegelin, A., Kretzschmar, R., 2009. Multi-metal contaminant dynamics in temporarily flooded soil under sulfate limitation. Geochim. Cosmochim. Acta 73 (19), 5513–5527. https://doi.org/10.1016/j.gca.2009.06.011.
Wu, S., Fang, G., Wang, Y., Zheng, Y., Wang, C., Zhao, F., Jaisi, D.P., Zhou, D.M., 2017. Redox-active oxygen-containing functional groups in activated carbon facilitate microbial reduction of ferrihydrite. Environ. Sci. Technol 51 (17), 9709–9717. https://doi.org/10.1021/acs.est7bb01854.
Xiao, Y., Zhang, E., Zhang, J.D., Dai, Y.F., Yang, Z.H., Christensen, H.E.M., Ulstrup, J., Zhao, F., 2017. Extracellular polymeric substances are transient media for microbial extracellular electron transfer. Sci. Adv. 3 (7), 77–82. https://doi.org/10.1126/sciadv.1700623.
Xu, S., Adhikari, D., Huang, R., Zhang, H., Tang, Y., Roden, E., Yang, Y., 2016. Biochar-facilitated microbial reduction of hematite. Environ. Sci. Technol. 50 (5), 2389–2395. https://doi.org/10.1021/acs.est.5b05517.
Ye, J., Zhang, R., Nielsen, S., Joseph, S.D., Huang, D., Thomas, T., 2016. A combination of biochar–mineral complexes and compost improves soil bacterial processes, soil quality, and plant properties. Front. Microbiol. 7, 372.
Yu, L., Yuan, Y., Tang, J., Wang, Y., Zhou, S., 2015. Biochar as an electron shuttle for reductive dechlorination of pentachlorophenol by *Geobacter sulfurreducens*. Sci. Rep. 5, 16221. https://doi.org/10.1038/srep16221.
Yuan, Y., Bolan, N., Prévoteau, A., Vithanage, M., Biswas, J.K., Ok, Y.S., Wang, H., 2017. Applications of biochar in redox-mediated reactions. Bioresour. Technol. 246, 271–281. https://doi.org/10.1016/j.biortech.2017.06.154.
Zachara, J.M., Fredrickson, J.K., Smith, S.C., Gassman, P.L., 2001. Solubilization of Fe(III) oxide-bound trace metals by a dissimilatory Fe(III) reducing bacterium. Geochim. Cosmochim. Acta 65 (1), 75–93. https://doi.org/10.1016/S0016-7037(00)00500-7.
Zhang, W., Niu, J.Z., Morales, V.L., Chen, X.C., Hay, A.G., Lehmann, J., Steenhuis, T.S., 2010. Transport and retention of biochar particles in agriculture soils contaminated by waste water and smelter dust. Ecohydrol 3, 497–508. https://doi.org/10.1002/eco.160.
Zhang, H.L., Fang, W., Wang, Y.P., Sheng, G.P., Zeng, R.J., Li, W.-W., Yu, H.-Q., 2013. Phosphorus removal in an enhanced biological phosphorus removal process: roles of extracellular. Environ. Sci. & Technol. 47 (20), 11482–11489 41. 10.1021.es303794d.
Zhou, G.W., Yang, X.R., Marshall, C.W., Li, H., Zheng, B.-X., Yan, Y., Su, J.-Q., Zhu, Y.-G., 2017. Biochar addition increases the rates of dissimilatory iron reduction and methanogenesis in ferrihydrite enrichments. Front. Microbiol. 8, 589. https://doi.org/10.3389/fmicbb.2017.00589.